

Asymptotic Modeling and Numerical Simulation of Solitary Waves in a Floating Ice Sheet

Philippe Guyenne¹, Emilian I. Părău²

¹ Department of Mathematical Sciences, University of Delaware, Newark, USA ²
School of Mathematics, University of East Anglia, Norwich, UK

ABSTRACT

Nonlinear flexural-gravity waves beneath a continuous ice sheet are considered. A Hamiltonian formulation of the governing equations is presented in the general three-dimensional setting. It is used to investigate the long-wave regime and derive an asymptotic model for weakly nonlinear dispersive waves with slower variation in the transverse direction. In the two-dimensional case, the model predictions are compared with direct numerical simulations of the full equations and a good agreement is found.

KEY WORDS: Boussinesq models; flexural-gravity waves; Hamiltonian systems; high-order spectral method; sea ice; solitary waves.

INTRODUCTION

In recent years, there has been renewed interest in the study of flexural-gravity (or hydroelastic) waves at the surface of a fluid covered by a thin elastic sheet, with applications to ocean waves interacting with sea ice in the polar regions (Korobkin et al., 2011). The recurrent interactions between ocean waves and sea ice are a prominent feature of these regions, and strongly affect sea-ice morphology and dynamics. A number of experiments have been performed with moving loads on ice, e.g. at McMurdo Sound, Antarctica, in deep water (Squire et al., 1996) and on Lake Saroma, Japan, in shallow water (Takizawa, 1985).

A theoretical challenge in this problem is to model the ice deformations subject to water wave motions, and thus a number of models have been proposed. The linear Euler–Bernoulli model for the ice sheet, combined with potential flow, has been widely used for small-amplitude water waves and ice deflections (Squire et al., 1996). However, reports of intense-in-ice events have highlighted limitations of linear theory (Marko, 2003) and, with the perspective of rougher sea conditions due to global warming (Squire, 2011; Kohout et al., 2014), nonlinear theory has drawn increasing attention.

Although polar sea ice does not actually form a continuous sheet, exhibiting many inhomogeneities such as cracks, leads and pressure ridges even in pack sea ice, or being fragmented as in the marginal ice zone, the present discussion will be centered on continuous sea-ice models. To a first approximation, it is of interest to investigate what nonlinear behavior is described by such models. These are primarily intended to simulate wave propagation in quasi-continuous pack sea ice far away from the open ocean. Large-amplitude (i.e. nonlinear) waves can potentially

travel long distances into the ice field. These models may be further justified in the present case by the fact that we focus on the long-wave regime and hence smaller-scale inhomogeneities of the ice sheet may be assumed to have little effect on the wave propagation.

In this context, nonlinear models based on Kirchhoff–Love plate theory have been adopted by a number of investigators, mostly in two dimensions. For example, Forbes (1986) computed periodic finite-amplitude waves using a Fourier series expansion technique. Părău and Dias (2002) derived a forced nonlinear Schrödinger equation for the envelope of ice-sheet deflections due to a moving load, and showed that solitary waves of elevation and depression exist for certain ranges of water depth. Bonnefoy et al. (2009) examined numerically the same nonlinear problem of moving load on ice, through a high-order spectral approach, and found a good agreement with theoretical predictions of Părău and Dias (2002). Hegarty and Squire (2008) simulated the interaction of large-amplitude water waves with a compliant floating raft such as a sea-ice floe, by expanding the solution as a series and evaluating it with a boundary-integral method.

Recently, Plotnikov and Toland (2011) proposed a nonlinear formulation based on the special Cosserat theory of hyperelastic shells, which has the advantage of conserving elastic energy unlike the Kirchhoff–Love model. In this Cosserat framework, Milewski et al. (2011, 2013) performed a weakly nonlinear modulational analysis of two- and three-dimensional hydroelastic waves on infinite and finite depth using the method of multiple scales. Guyenne and Părău (2012, 2014) examined the two-dimensional problem through a Hamiltonian reformulation of the governing equations. On this basis, they analyzed both the modulational and long-wave limits, and compared their asymptotic results with direct numerical simulations.

The present study extends the work of Guyenne and Părău (2014) to the three-dimensional case. As a starting point, we take advantage of the conservative property of the Cosserat formulation to express the governing equations of the three-dimensional hydroelastic problem in Hamiltonian form, thus extending Zakharov’s Hamiltonian formulation for nonlinear water waves to flexural-gravity waves. In doing so, the Dirichlet–Neumann operator (DNO) is introduced to reduce the original Laplace problem to a lower-dimensional system involving quantities evaluated only at the fluid-ice interface. Similarly to Haragus-Courcelle and Ilichev (1998) and Xia and Shen (2002), we then focus on the long-wave regime and establish a high-order Kadomtsev–Petviashvili (KP) equation for weakly three-dimensional nonlinear dispersive waves on finite depth. To this aim, we use the Hamiltonian perturbation approach

of Craig et al. (2005a,b), which is well-suited to the present Hamiltonian formulation. The derivation of this high-order KP equation is a new theoretical accomplishment and constitutes the main result of our paper. We note incidentally that Xia and Shen (2002) proposed a 5th-order Korteweg–de Vries (KdV) equation for two-dimensional hydroelastic waves on shallow water in the linear Euler–Bernoulli case, and Haragus-Courcelle and Ilichev (1998) derived a three-dimensional generalization of the 5th-order KdV equation in a similar setting.

When restricted to two dimensions, our long-wave model also reduces to a 5th-order KdV equation and its predictions are compared with direct numerical simulations of the full equations. Such simulations allow for a more detailed investigation over a wider range of parameter values. In particular, thanks to its analyticity properties, the DNO has a convergent Taylor series expansion in which each term can be determined recursively. This series expansion combined with the fast Fourier transform leads to an efficient and accurate numerical scheme for solving the full Hamiltonian equations. Guyenne and Părău (2014) computed solitary waves of both depression and elevation, including overturning waves of depression for sufficiently low speeds and large depth. Solitary waves of depression were found to be stable while solitary waves of elevation seem to be unstable. In the shallow-water limit, these solitary waves of elevation resemble generalized solitary wave solutions of the 5th-order KdV equation, and were observed to persist for long times. They however are inherently unstable because they continuously emit radiation and thus decay in time. We also review some of these numerical results in the present paper.

In the following sections, we present the mathematical formulation of the hydroelastic problem. The DNO is introduced and the Hamiltonian equations of motion are established. From this Hamiltonian formulation, weakly nonlinear wave models are derived in the long-wave limit. Direct numerical simulations are then shown to assess and complement these asymptotic results.

MATHEMATICAL FORMULATION

Equations of Motion

We consider a three-dimensional fluid of uniform finite depth h beneath a continuous thin ice sheet. The fluid is assumed to be incompressible and inviscid, and the flow to be irrotational. The ice sheet is modeled using the special Cosserat theory of hyperelastic shells in Cartesian coordinates (x, y, z) , with the horizontal (x, y) -plane being the bottom of the ice sheet at rest and the z -axis directed vertically upwards. The vertical deformation of the ice is denoted by $z = \eta(x, y, t)$. The fluid velocity potential $\Phi(x, y, z, t)$ satisfies the Laplace equation

$$\nabla^2 \Phi = 0, \quad \text{for } \vec{x} = (x, y)^\top \in \mathbb{R}^2, \quad -h < z < \eta(x, y, t). \quad (1)$$

The nonlinear boundary conditions at $z = \eta(x, y, t)$ are the kinematic condition

$$\eta_t + \Phi_x \eta_x + \Phi_y \eta_y = \Phi_z, \quad (2)$$

and the dynamic condition

$$\Phi_t + \frac{1}{2} |\nabla \Phi|^2 + g\eta + \frac{\mathcal{D}}{\rho} \mathcal{F} = 0, \quad (3)$$

where

$$\begin{aligned} \mathcal{F} = & \frac{2}{\sqrt{\mathcal{A}}} \left[\partial_x \left(\frac{1+\eta_x^2}{\sqrt{\mathcal{A}}} \partial_x \mathcal{H} \right) - \partial_x \left(\frac{\eta_x \eta_y}{\sqrt{\mathcal{A}}} \partial_y \mathcal{H} \right) - \partial_y \left(\frac{\eta_x \eta_y}{\sqrt{\mathcal{A}}} \partial_x \mathcal{H} \right) \right. \\ & \left. + \partial_y \left(\frac{1+\eta_y^2}{\sqrt{\mathcal{A}}} \partial_y \mathcal{H} \right) \right] + 4\mathcal{H}^3 - 4\mathcal{H} \mathcal{H}', \end{aligned}$$

with

$$\mathcal{A} = 1 + \eta_x^2 + \eta_y^2, \quad \mathcal{K} = \frac{1}{\mathcal{A}^2} (\eta_{xx} \eta_{yy} - \eta_{xy}^2),$$

$$\mathcal{H} = \frac{1}{2\mathcal{A}^{3/2}} \left[(1 + \eta_y^2) \eta_{xx} - 2\eta_{xy} \eta_x \eta_y + (1 + \eta_x^2) \eta_{yy} \right].$$

The additional term \mathcal{F} in (3) represents the nonlinear bending force exerted by the ice sheet onto the fluid surface, as derived by Plotnikov and Toland (2011). It is also a conservative term and thus can be cast into a Hamiltonian formulation as shown below. Note that \mathcal{A} , \mathcal{K} and \mathcal{H} denote respectively the squared normal vector norm, Gaussian curvature and mean curvature at any point on the ice sheet. Two simpler expressions of this bending force have been commonly used in the literature; a linear one based on Euler–Bernoulli theory (Squire et al., 1996; Haragus-Courcelle and Ilichev, 1998; Părău and Vanden-Broeck, 2011),

$$\mathcal{F} = \eta_{xxxx} + 2\eta_{xxyy} + \eta_{yyyy},$$

and a nonlinear one based on Kirchhoff–Love theory (Forbes, 1986; Părău and Dias, 2002; Bonnefoy et al., 2009; Milewski et al., 2011). The system is completed with the boundary condition at the bottom,

$$\Phi_z = 0 \quad \text{at } z = -h. \quad (4)$$

Hereinafter, subscripts are also used as short notation for partial or variational derivatives (e.g. $\Phi_t = \partial_t \Phi$). The constant \mathcal{D} is the coefficient of flexural rigidity for the ice sheet, ρ the density of the fluid and g the acceleration due to gravity. The dynamic condition (3) is obtained from the Bernoulli equation. The inertia of the thin elastic plate is neglected, so the plate acceleration term is not considered here. We also assume that the elastic plate is not pre-stressed and neglect plate stretching.

The dispersion relation for the linearized problem with solutions of the form $e^{i(\vec{k}\vec{x} - \omega t)}$ is

$$c^2 = \left(\frac{g}{k} + \frac{\mathcal{D}k^3}{\rho} \right) \tanh(hk), \quad (5)$$

where $k = |\vec{k}|$ and $c = \omega/k$ is the phase speed. It can be shown that the phase speed $c(\vec{k})$ has a minimum c_{\min} at $\vec{k} = \vec{k}_{\min}$ for any parameter values (Squire et al., 1996; Părău and Dias, 2002). At this minimum, the phase velocity and group velocity are equal. Another critical speed in finite depth is the long-wave (or shallow-water) limit $c_0 = \sqrt{gh}$ as $k \rightarrow 0$. The present study focuses on solitary wave solutions propagating at speeds near c_0 .

The total energy

$$H = \frac{1}{2} \iint_{-\infty}^{\infty} \int_{-h}^{\eta} |\nabla \Phi|^2 dz dy dx + \frac{1}{2} \iint_{-\infty}^{\infty} \left[g\eta^2 + 4\frac{\mathcal{D}}{\rho} \mathcal{H}^2 \sqrt{\mathcal{A}} \right] dy dx, \quad (6)$$

together with the impulse (or momentum) vector

$$I = \iint_{-\infty}^{\infty} \int_{-h}^{\eta} \nabla_{\vec{x}} \Phi dz dy dx,$$

where $\nabla_{\vec{x}} = (\partial_x, \partial_y)^\top$, and the volume (or mass)

$$V = \iint_{-\infty}^{\infty} \eta dy dx,$$

are invariants of motion for (1)–(4). The first integral in (6) represents kinetic energy, while the second integral represents potential energy due to gravity and elasticity.

Hamiltonian Formulation

Following Zakharov (1968) and Craig and Sulem (1993), we can reduce the dimensionality of the Laplace problem (1)~(4) by introducing $\xi(x, y, t) = \Phi(x, y, \eta(x, y, t), t)$, the trace of the velocity potential on $z = \eta(x, y, t)$, together with the DNO

$$G(\eta)\xi = (-\nabla_{\bar{x}}\eta, 1)^\top \cdot \nabla\Phi|_{z=\eta},$$

which is the singular integral operator that takes Dirichlet data ξ on $z = \eta(x, y, t)$, solves the Laplace equation (1) for Φ subject to (4), and returns the corresponding Neumann data (i.e. the normal fluid velocity there).

In terms of these boundary variables, the equations of motion take the canonical form

$$\begin{pmatrix} \eta_t \\ \xi_t \end{pmatrix} = J \begin{pmatrix} H_\eta \\ H_\xi \end{pmatrix} = \begin{pmatrix} 0 & 1 \\ -1 & 0 \end{pmatrix} \begin{pmatrix} H_\eta \\ H_\xi \end{pmatrix}, \quad (7)$$

where the 2×2 matrix J represents the symplectic structure of the system. More specifically,

$$\begin{aligned} \eta_t &= G(\eta)\xi, \\ \xi_t &= -\frac{1}{2(1+|\nabla_{\bar{x}}\eta|^2)} \left[|\nabla_{\bar{x}}\xi|^2 - (G(\eta)\xi)^2 - 2(G(\eta)\xi)\nabla_{\bar{x}}\xi \cdot \nabla_{\bar{x}}\eta \right. \\ &\quad \left. + |\nabla_{\bar{x}}\xi|^2 |\nabla_{\bar{x}}\eta|^2 - (\nabla_{\bar{x}}\xi \cdot \nabla_{\bar{x}}\eta)^2 \right] - g\eta - \frac{\mathcal{D}}{\rho} \mathcal{F}, \end{aligned} \quad (8)$$

which are Hamiltonian equations for the canonically conjugate variables η and ξ , extending Zakharov's formulation of the water wave problem to flexural-gravity waves (Guyenne and Părău, 2012; 2014). The Hamiltonian is given by

$$H = \frac{1}{2} \iint_{-\infty}^{\infty} \left[\xi G(\eta)\xi + g\eta^2 + \frac{4\mathcal{D}}{\rho} \mathcal{H}^2 \sqrt{\mathcal{A}} \right] dy dx, \quad (10)$$

and corresponds to the total energy (6).

Dirichlet–Neumann Operator

In light of its analyticity properties (Craig et al., 1997), the DNO can be expressed as a convergent Taylor series expansion in η ,

$$G(\eta) = \sum_{j=0}^{\infty} G_j(\eta), \quad (11)$$

where each term G_j can be determined recursively (Craig and Sulem, 1993; Xu and Guyenne, 2009). The resulting expressions are identical to those in the context of water waves. More specifically, for $j = 2r > 0$,

$$\begin{aligned} G_{2r}(\eta) &= \frac{1}{(2r)!} G_0(|D_{\bar{x}}|^2)^{r-1} D_{\bar{x}} \cdot \eta^{2r} D_{\bar{x}} \\ &\quad - \sum_{s=0}^{r-1} \frac{1}{(2(r-s))!} (|D_{\bar{x}}|^2)^{r-s} \eta^{2(r-s)} G_{2s}(\eta) \\ &\quad - \sum_{s=0}^{r-1} \frac{1}{(2(r-s-1))!} G_0(|D_{\bar{x}}|^2)^{r-s-1} \eta^{2(r-s-1)} G_{2s+1}(\eta), \end{aligned} \quad (12)$$

and, for $j = 2r - 1 > 0$,

$$\begin{aligned} G_{2r-1}(\eta) &= \frac{1}{(2r-1)!} (|D_{\bar{x}}|^2)^{r-1} D_{\bar{x}} \cdot \eta^{2r-1} D_{\bar{x}} \\ &\quad - \sum_{s=0}^{r-1} \frac{1}{(2(r-s)-1)!} G_0(|D_{\bar{x}}|^2)^{r-s-1} \eta^{2(r-s)-1} G_{2s}(\eta) \\ &\quad - \sum_{s=0}^{r-2} \frac{1}{(2(r-s-1))!} (|D_{\bar{x}}|^2)^{r-s-1} \eta^{2(r-s-1)} G_{2s+1}(\eta), \end{aligned} \quad (13)$$

where $D_{\bar{x}} = -i\nabla_{\bar{x}}$ and $G_0 = |D_{\bar{x}}| \tanh(h|D_{\bar{x}}|)$ are Fourier multiplier operators ($D_{\bar{x}}$ is defined in such a way that its Fourier symbol is \vec{k} and thus $|D_{\bar{x}}|$ corresponds to $|\vec{k}| = k$). In the infinite-depth limit ($h \rightarrow \infty$), G_0 reduces to $|D_{\bar{x}}|$. For example, the first terms of up to second order in η read

$$\begin{aligned} G_1(\eta) &= D_{\bar{x}}\eta \cdot D_{\bar{x}} - G_0\eta G_0, \\ G_2(\eta) &= -\frac{1}{2} \left(|D_{\bar{x}}|^2 \eta^2 G_0 + G_0 \eta^2 |D_{\bar{x}}|^2 - 2G_0\eta G_0\eta G_0 \right). \end{aligned}$$

This series expansion of the DNO will play a central role in the present asymptotic and numerical procedures, as discussed in the next sections. Such a formulation involving the DNO and boundary variables alone is advantageous compared to a volumetric approach which requires explicitly solving for the entire domain (e.g. in finite-element methods). It has also been successfully used in other contexts, e.g. in perturbation calculations for surface gravity waves in single- and double-layer fluids (Craig et al., 2005a,b; 2012), as well as in direct numerical simulations with uniform or variable water depth (Craig and Sulem, 1993; Guyenne and Nicholls, 2007; Xu and Guyenne, 2009).

LONG-WAVE REGIME

In this section, we analyze the weakly nonlinear regime for small-to moderate-amplitude waves on a three-dimensional fluid of finite depth. Following Haragus-Courcelle and Ilchev (1998) and Xia and Shen (2002), we focus on the long-wave regime for wave speeds near c_0 . We emphasize that these previous studies considered simpler models for the ice sheet and employed different methods to derive their asymptotic wave models. Here we apply the Hamiltonian perturbation approach of Craig et al. (2005a,b), which is especially suitable for the present Hamiltonian formulation of the hydroelastic problem. An advantage of this approach is that it naturally associates a Hamiltonian to the equations of motion at each order of approximation. Changing variables through canonical transformations and expanding the Hamiltonian (10) are the key ingredients. Below we only present the main steps in the derivation of our weakly nonlinear models and refer the reader to Craig et al. (2005a,b) for further details about the approach.

Boussinesq System

As a starting point, we introduce the long-wave scalings

$$X = \varepsilon x, Y = \varepsilon^2 y, \eta(x, y, t) = \varepsilon^2 \tilde{\eta}(X, Y, t), \xi(x, y, t) = \varepsilon \tilde{\xi}(X, Y, t), \quad (14)$$

where the small parameter $\varepsilon^2 \sim (h/\ell_0)^2 \sim a_0/h \ll 1$ is a measure of weak dispersion and nonlinearity (with a_0 and ℓ_0 being a characteristic wave height and wavelength respectively). The different scalings in x and y reflect the choice that the variations in y are slower than in x (the solution traveling primarily in the x -direction) in anticipation to a KP equation. Inserting (14) in the Hamiltonian (10) and expanding it in powers of ε up to order $O(\varepsilon^5)$, we find

$$\begin{aligned} H &= \frac{\varepsilon}{2} \iint_{-\infty}^{\infty} \left[h \tilde{\xi}_{\bar{x}}^2 + g \tilde{\eta}^2 + \varepsilon^2 \left(h \tilde{\xi}_{\bar{y}}^2 - \frac{h^3}{3} \tilde{\xi}_{\bar{x}\bar{x}}^2 + \tilde{\eta} \tilde{\xi}_{\bar{x}}^2 \right) \right. \\ &\quad \left. + \varepsilon^4 \left(\frac{2}{15} h^5 \tilde{\xi}_{\bar{x}\bar{x}\bar{x}}^2 - \frac{2}{3} h^3 \tilde{\xi}_{\bar{x}\bar{x}} \tilde{\xi}_{\bar{y}\bar{y}} + \tilde{\eta} \tilde{\xi}_{\bar{y}}^2 \right. \right. \\ &\quad \left. \left. - h^2 \tilde{\eta} \tilde{\xi}_{\bar{x}\bar{x}}^2 + \frac{\mathcal{D}}{\rho} \tilde{\eta}_{\bar{x}\bar{x}}^2 \right) \right] dY dX + O(\varepsilon^7). \end{aligned} \quad (15)$$

To obtain this approximation, it is sufficient to only retain G_0 and G_1 in (11). It is also common in the long-wave regime to use some velocity as a dependent variable, rather than the velocity potential. Defining

$$u = \tilde{\xi}_X, \quad (16)$$

which plays the role of a horizontal velocity in the X -direction (hence

$\tilde{\xi} = \partial_X^{-1} u$, the Hamiltonian (15) becomes

$$H = \frac{\varepsilon}{2} \iint_{-\infty}^{\infty} \left[hu^2 + g\tilde{\eta}^2 + \varepsilon^2 \left(h(\partial_X^{-1} u_Y)^2 - \frac{h^3}{3} u_{XX}^2 + \tilde{\eta} u^2 \right) + \varepsilon^4 \left(\frac{2}{15} h^5 u_{XXX}^2 - \frac{2}{3} h^3 u_X (\partial_X^{-1} u_{YY}) + \tilde{\eta} (\partial_X^{-1} u_Y)^2 - h^2 \tilde{\eta} u_X^2 + \frac{\mathcal{D}}{\rho} \tilde{\eta}_{XX}^2 \right) \right] dY dX + O(\varepsilon^7).$$

There is also a change in symplectic form associated with these transformations. The new dependent variables in (14) can be expressed as $(\tilde{\eta}, \tilde{\xi})^\top = A_1(\eta, \xi)^\top$ in terms of

$$A_1 = \begin{pmatrix} \varepsilon^{-2} & 0 \\ 0 & \varepsilon^{-1} \end{pmatrix},$$

so that Eqs. (7) are transformed to

$$\begin{pmatrix} \tilde{\eta}_t \\ \tilde{\xi}_t \end{pmatrix} = J_1 \begin{pmatrix} H_{\tilde{\eta}} \\ H_{\tilde{\xi}} \end{pmatrix} = \begin{pmatrix} 0 & 1 \\ -1 & 0 \end{pmatrix} \begin{pmatrix} H_{\tilde{\eta}} \\ H_{\tilde{\xi}} \end{pmatrix},$$

where $J_1 = \varepsilon^3 A_1 J A_1^\top$, the extra factor ε^3 stemming from the spatial rescaling $\vec{x} = (x, y)^\top \rightarrow \vec{X} = (X, Y)^\top = (\varepsilon x, \varepsilon^2 y)^\top$. Then using the matrix form

$$\begin{pmatrix} \tilde{\eta} \\ u \end{pmatrix} = A_2 \begin{pmatrix} \tilde{\eta} \\ \tilde{\xi} \end{pmatrix} = \begin{pmatrix} 1 & 0 \\ 0 & \partial_X \end{pmatrix} \begin{pmatrix} \tilde{\eta} \\ \tilde{\xi} \end{pmatrix},$$

of (16) leads to

$$\begin{pmatrix} \tilde{\eta}_t \\ u_t \end{pmatrix} = J_2 \begin{pmatrix} H_{\tilde{\eta}} \\ H_u \end{pmatrix} = \begin{pmatrix} 0 & -\partial_X \\ -\partial_X & 0 \end{pmatrix} \begin{pmatrix} H_{\tilde{\eta}} \\ H_u \end{pmatrix},$$

where $J_2 = A_2 J_1 A_2^\top$. These equations constitute a high-order Boussinesq system in the present problem and read more explicitly

$$\begin{aligned} \eta_\tau &= -hu_X - \varepsilon^2 \left(h\partial_X^{-1} u_{YY} + \frac{h^3}{3} u_{XXX} + (\eta u)_X \right) \\ &\quad - \varepsilon^4 \left(\frac{2}{15} h^5 u_{XXXXX} + \frac{2}{3} h^3 u_{XYY} + (\eta \partial_X^{-1} u_Y)_Y + h^2 (\eta u_X)_{XX} \right), \\ u_\tau &= -g\eta_X - \varepsilon^2 uu_X - \varepsilon^4 \left(u_Y (\partial_X^{-1} u_Y) - h^2 u_X u_{XX} + \frac{\mathcal{D}}{\rho} \eta_{XXXXX} \right), \end{aligned}$$

after dropping the tildes, where $\tau = \varepsilon t$ is a long time scale. Retaining terms of up to order $O(\varepsilon^2)$ and neglecting the Y -dependence, this yields the well-known integrable Kaup–Boussinesq system of the water wave problem without flexural effects (Kaup, 1975), namely

$$\begin{aligned} \eta_\tau &= -hu_X - \varepsilon^2 \left(\frac{h^3}{3} u_{XXX} + (\eta u)_X \right), \\ u_\tau &= -g\eta_X - \varepsilon^2 uu_X. \end{aligned}$$

High-Order KP Equation

Furthermore, by framing the Boussinesq system in characteristic coordinates

$$\begin{pmatrix} r \\ s \end{pmatrix} = A_3 \begin{pmatrix} \eta \\ u \end{pmatrix} = \begin{pmatrix} \left(\frac{g}{4h}\right)^{1/4} & \left(\frac{h}{4g}\right)^{1/4} \\ \left(\frac{g}{4h}\right)^{1/4} & -\left(\frac{h}{4g}\right)^{1/4} \end{pmatrix} \begin{pmatrix} \eta \\ u \end{pmatrix}, \quad (17)$$

we obtain

$$\begin{aligned} H &= \frac{\varepsilon}{2} \iint_{-\infty}^{\infty} \left[\sqrt{gh}(r^2 + s^2) + \varepsilon^2 \left\{ \frac{1}{2} \sqrt{gh} \left((\partial_X^{-1} r_Y)^2 - 2(\partial_X^{-1} r_Y)(\partial_X^{-1} s_Y) + (\partial_X^{-1} s_Y)^2 \right) - \frac{h^2}{6} \sqrt{gh} \left(r_X^2 - 2r_X s_X + s_X^2 \right) + \frac{1}{2\sqrt{2}} \left(\frac{g}{h} \right)^{1/4} (r^3 - r^2 s - r s^2 + s^3) \right\} + \varepsilon^4 \left\{ \frac{h^4}{15} \sqrt{gh} \left(r_{XX}^2 - 2r_{XX} s_{XX} + s_{XX}^2 \right) - \frac{h^2}{3} \sqrt{gh} \left(r_X (\partial_X^{-1} r_{YY}) - r_X (\partial_X^{-1} s_{YY}) - s_X (\partial_X^{-1} r_{YY}) + s_X (\partial_X^{-1} s_{YY}) \right) + \frac{1}{2\sqrt{2}} \left(\frac{g}{h} \right)^{1/4} \left(r (\partial_X^{-1} r_Y)^2 - 2r (\partial_X^{-1} r_Y) (\partial_X^{-1} s_Y) + r (\partial_X^{-1} s_Y)^2 + s (\partial_X^{-1} r_Y)^2 - 2s (\partial_X^{-1} r_Y) (\partial_X^{-1} s_Y) + s (\partial_X^{-1} s_Y)^2 \right) - \frac{h^2}{2\sqrt{2}} \left(\frac{g}{h} \right)^{1/4} \left(r r_X^2 - 2r r_X s_X + r s_X^2 + s r_X^2 - 2s r_X s_X + s s_X^2 \right) + \frac{\mathcal{D}}{2\rho} \sqrt{\frac{h}{g}} \left(r_{XX}^2 + 2r_{XX} s_{XX} + s_{XX}^2 \right) \right\} \right] dY dX + O(\varepsilon^7), \quad (18) \end{aligned}$$

where r and s are principally right- and left-moving components of the solution in the X -direction respectively, which obey the evolution equations

$$\begin{pmatrix} r_t \\ s_t \end{pmatrix} = J_3 \begin{pmatrix} H_r \\ H_s \end{pmatrix} = \begin{pmatrix} -\partial_X & 0 \\ 0 & \partial_X \end{pmatrix} \begin{pmatrix} H_r \\ H_s \end{pmatrix}.$$

This transformation to characteristic coordinates is also accompanied by a change in symplectic form, with $J_3 = A_3 J_2 A_3^\top$. The Hamiltonian (18) can be further reduced by subtracting a scalar multiple of the conserved impulse,

$$\mathcal{C} \cdot I = \iint_{-\infty}^{\infty} \eta (\mathcal{C} \cdot \nabla_{\vec{x}} \xi) dy dx = \frac{\varepsilon}{2} \iint_{-\infty}^{\infty} \sqrt{gh}(r^2 - s^2) dY dX,$$

where $\mathcal{C} = (c_0, 0)^\top$, and by restricting our attention to right-moving solutions r in a region of phase space where $s \leq O(\varepsilon^3)$. As a result, the new Hamiltonian takes the form

$$\begin{aligned} \tilde{H} &= H - \mathcal{C} \cdot I, \\ &= \frac{\varepsilon^3}{2} \iint_{-\infty}^{\infty} \left[\frac{1}{2} \sqrt{gh} (\partial_X^{-1} r_Y)^2 - \frac{h^2}{6} \sqrt{gh} r_X^2 + \frac{1}{2\sqrt{2}} \left(\frac{g}{h} \right)^{1/4} r^3 + \varepsilon^2 \left\{ \left(\frac{h^4}{15} \sqrt{gh} + \frac{\mathcal{D}}{2\rho} \sqrt{\frac{h}{g}} \right) r_{XX}^2 - \frac{h^2}{3} \sqrt{gh} r_X (\partial_X^{-1} r_{YY}) + \frac{1}{2\sqrt{2}} \left(\frac{g}{h} \right)^{1/4} r (\partial_X^{-1} r_Y)^2 - \frac{h^2}{2\sqrt{2}} \left(\frac{g}{h} \right)^{1/4} r r_X^2 \right\} \right] dY dX + O(\varepsilon^7), \end{aligned}$$

and the evolution equation for r becomes

$$r_t = -\partial_X \tilde{H}_r,$$

which is expressed in a reference frame moving at speed $c_0 = \sqrt{gh}$ in the X -direction (as a result of the subtraction of $\mathcal{C} \cdot I$ from H). More explicitly, this yields the high-order KP equation

$$\begin{aligned} r_\tau + c_1 \partial_X^{-1} r_{YY} + 3c_2 r r_X + c_3 r_{XXX} + \varepsilon^2 c_2 \left(2r_Y (\partial_X^{-1} r_Y) + r (\partial_X^{-1} r_{YY}) \right) + 2\varepsilon^2 c_3 r_{XYY} + \varepsilon^2 c_4 (2r_X r_{XX} + r r_{XXX}) + \varepsilon^2 c_5 r_{XXXXX} &= 0, \quad (19) \end{aligned}$$

where $\tau = \varepsilon^3 t$ and

$$c_1 = \frac{1}{2} \sqrt{gh}, \quad c_2 = \frac{1}{2\sqrt{2}} \left(\frac{g}{h} \right)^{1/4}, \quad c_3 = \frac{h^2}{6} \sqrt{gh},$$

$$c_4 = \frac{h^2}{2\sqrt{2}} \left(\frac{g}{h}\right)^{1/4}, \quad c_5 = \frac{h^4}{15} \sqrt{gh} + \frac{\mathcal{D}}{2\rho} \sqrt{\frac{h}{g}}.$$

Note that the coefficients c_1, \dots, c_5 are all positive. The corresponding Hamiltonian (with respect to τ) is given by

$$H = \frac{1}{2} \iint_{-\infty}^{\infty} \left[c_1 (\partial_X^{-1} r_Y)^2 + c_2 r^3 - c_3 r_X^2 + \varepsilon^2 c_2 r (\partial_X^{-1} r_Y)^2 - 2\varepsilon^2 c_3 r_X (\partial_X^{-1} r_{YY}) - \varepsilon^2 c_4 r r_X^2 + \varepsilon^2 c_5 r_{XX}^2 \right] dY dX.$$

To lowest order by neglecting the $O(\varepsilon^2)$ terms, Eq. (19) reduces to the KP-II equation for three-dimensional surface gravity waves, which admits solutions called line solitons of the form

$$r(\vec{p} \cdot \vec{X} + q\tau) = \frac{c_3}{c_2} (\ell_1 - \ell_2)^2 \operatorname{sech}^2 \left[\frac{1}{2} (\vec{p} \cdot \vec{X} + q\tau) \right],$$

where

$$\vec{p} = (p_1, p_2)^\top = (\ell_1 - \ell_2, \ell_1^2 - \ell_2^2)^\top, \quad q = 4c_3(\ell_1^3 - \ell_2^3),$$

and $\ell_1, \ell_2 \in \mathbb{R}$ (Biondini and Chakravarty, 2006).

5th-Order KdV Equation

In the two-dimensional case (no Y -variation), Eq. (19) turns into the 5th-order KdV equation

$$r_\tau + 3c_2 r r_X + c_3 r_{XXX} + 2\varepsilon^2 c_4 r_X r_{XX} + \varepsilon^2 c_4 r r_{XXX} + \varepsilon^2 c_5 r_{XXXXX} = 0, \quad (20)$$

with Hamiltonian (with respect to τ)

$$H = \frac{1}{2} \int_{-\infty}^{\infty} \left[c_2 r^3 - c_3 r_X^2 - \varepsilon^2 c_4 r r_X^2 + \varepsilon^2 c_5 r_{XX}^2 \right] dX.$$

This Hamiltonian 5th-order KdV equation is similar to those investigated by Craig and Groves (1994) and Champneys et al. (2002) in the context of gravity and capillary-gravity water waves, respectively. However, there are noticeable differences from the 5th-order KdV equations derived by Haragus-Courcelle and Ilichev (1998) and Xia and Shen (2002) for flexural-gravity waves, which do not have the high-order nonlinear terms in factor of c_4 .

Particular attention will be paid to Eq. (20) in the present study. Because this equation is not exactly integrable in general, it is solved numerically for solitary waves which are stationary in a secondary reference frame moving at constant speed σ . In our Hamiltonian framework, these solutions correspond to fixed points of the variational $\delta_r(H - \sigma I)$. This leads to the nonlinear ordinary differential equation

$$-\sigma r + \frac{3}{2} c_2 r^2 + c_3 r_{XX} + \varepsilon^2 c_4 (r r_X)_X - \frac{\varepsilon^2}{2} c_4 r_X^2 + \varepsilon^2 c_5 r_{XXXXX} = 0, \quad (21)$$

which is discretized by a pseudospectral method assuming periodic boundary conditions. Equation (21) is solved iteratively by Newton's method using the classical KdV soliton

$$r(X) = \frac{\sigma}{c_2} \operatorname{sech}^2 \left(\frac{1}{2} \sqrt{\frac{\sigma}{c_3}} X \right), \quad (22)$$

as an initial guess. A number of 1024 grid points is typically specified in these computations. Results will be presented in the next section.

At this order of approximation, the ice-sheet deflection is given in terms of r by

$$\eta = \left(\frac{h}{4g} \right)^{1/4} r, \quad (23)$$

after inverting (17) and neglecting the smaller contribution from s . Note that the unscaled variables (14) should eventually be reintroduced in order to compare with direct numerical simulations.

DIRECT NUMERICAL SIMULATIONS

In this section, we perform two-dimensional, direct numerical simulations of (1)~(4) to illustrate general properties of the mathematical formulation and test predictions from our weakly nonlinear model (20). Computations of both steady (in a moving frame) and time-dependent solutions are discussed.

Numerical Methods

Following Takizawa (1985), Bonnefoy et al. (2009) and Milewski et al. (2011), we non-dimensionalize the equations using the characteristic scales

$$\mathcal{L} = \left(\frac{\mathcal{D}}{\rho g} \right)^{1/4}, \quad \mathcal{V} = \left(\frac{\mathcal{D} g^3}{\rho} \right)^{1/8},$$

as unit length and unit velocity, respectively. In the two-dimensional setting, the x -axis now refers to the horizontal direction while the y -axis refers to the vertical direction. Since we are interested in solitary waves, the key parameters to be examined are the dimensionless wave speed c and the dimensionless water depth h . We will pay particular attention to the case $h = 3.095$ which corresponds to Takizawa's experiments on Lake Saroma, Japan.

To compute fully nonlinear steady and unsteady waves, we use a boundary-integral method (combined with Cauchy's integral formula) and a high-order spectral method, respectively. A brief description of these numerical methods is presented below and the reader is referred to Guyenne and Părău (2012, 2014) for further details.

For steady waves in a reference frame moving at constant speed c , the complex potential

$$w(z) = \Phi(x, y) + i\Psi(x, y),$$

is introduced in the fluid domain, where $\Psi(x, y)$ is the stream function. The physical plane

$$z = x(w) + iy(w),$$

is mapped to $w(z)$ in the inverse plane. Therefore

$$\Phi_x - i\Phi_y = \frac{dw}{dz} = \frac{1}{x_\Phi + iy_\Phi}.$$

Without loss of generality, we set $\Psi = 0$ on the fluid-ice interface and choose $\Phi = 0$ at $x = 0$. It can be shown that $\Psi = -ch$ on the bottom. In terms of the potential, the fluid-ice interface is parameterized by

$$(x(\Phi), y(\Phi)) = (x(\Phi + i0), y(\Phi + i0)).$$

In this notation, $x'(\Phi)$ and $y'(\Phi)$ are the values of x_Φ and y_Φ evaluated at the interface $\Psi = 0$. As $y_\Phi = 0$ on the bottom $\Psi = -ch$, we can extend the function $x_\Phi - 1/c + iy_\Phi$ by symmetry about the line $\Psi = -ch$ to an analytic function in the strip $(-2ch, 0)$.

We apply Cauchy's integral formula along a rectangular strip between $\Psi = 0$ and $\Psi = -2ch$. Assuming the symmetry of solutions about $\Phi = 0$, application of Cauchy's integral formula yields, after some algebra,

$$x'(\Phi_0) - \frac{1}{c} = -\frac{1}{\pi} \int_0^\infty y'(\Phi) \left(\frac{1}{\Phi - \Phi_0} + \frac{1}{\Phi + \Phi_0} \right) d\Phi$$

$$\begin{aligned}
& + \frac{1}{\pi} \int_0^\infty \frac{(\Phi_0 - \Phi)y'(\Phi) + 2ch(x'(\Phi) - 1/c)}{(\Phi - \Phi_0)^2 + 4c^2h^2} d\Phi \\
& + \frac{1}{\pi} \int_0^\infty \frac{-(\Phi_0 + \Phi)y'(\Phi) + 2ch(x'(\Phi) - 1/c)}{(\Phi + \Phi_0)^2 + 4c^2h^2} d\Phi, \quad (24)
\end{aligned}$$

where the primes denote differentiation with respect to Φ . The evaluation point Φ_0 lies on the interface and the first integral on the right-hand side is evaluated in the principal-value sense. A typical resolution $\Delta\Phi = 0.025$ is used in the quadrature of (24). Thanks to the hodograph transformation, this numerical method can handle multivalued solutions. However, it is especially designed for computing solitary waves and thus is not suitable for periodic waves in general.

To compute unsteady waves, we directly solve the Hamiltonian equations (8)~(9) in space and time (Guyenne and Nicholls, 2007). For space discretization, we assume periodic boundary conditions in x , with $0 \leq x \leq L$, and use a pseudospectral method based on the fast Fourier transform. This is a particularly suitable choice for the computation of the DNO since each term in its Taylor series expansion (11)~(13) consists of concatenations of Fourier multipliers with powers of η . More specifically, both functions η and ξ are expanded in truncated Fourier series

$$\begin{pmatrix} \eta \\ \xi \end{pmatrix} = \sum_k \begin{pmatrix} \hat{\eta}_k \\ \hat{\xi}_k \end{pmatrix} e^{ikx}.$$

Spatial derivatives and Fourier multipliers are evaluated in the Fourier domain, while nonlinear products are calculated in the physical domain on a regular grid of N collocation points. In practice, the Taylor series of the DNO is also truncated to a finite number of terms,

$$G(\eta) \approx \sum_{j=0}^M G_j(\eta), \quad (25)$$

but thanks to its analyticity properties, a small number of terms (typically $M < 10$) is sufficient to achieve very accurate results (Xu and Guyenne, 2009).

Time integration of (8) and (9) is performed in the Fourier domain so that the linear terms can be solved exactly by the integrating factor technique. The nonlinear terms are integrated in time using a 4th-order Runge–Kutta scheme with constant time step Δt . Starting from zero initial conditions, solitary waves are produced by applying the localized pressure

$$P = P_0 e^{-(x-x_0-ct)^2/16}, \quad (26)$$

over a finite interval of time $0 \leq t \leq T$, with given P_0 and c ($T = 125$ is chosen in all of our time-dependent simulations). The pressure term (26) is added to the right-hand side of (9) and its distribution is initially centered at $x_0 = L/2$. To minimize the generation of radiation due to a cold start, we also apply a tanh-like ramp function in time to (26), which allows for a smooth transition from 0 to P_0 . Despite our effort however, small radiative waves were inevitably excited by the applied pressure in our numerical simulations.

A typical run uses $M = 6$, $\Delta t = 0.002$ and $N = 4096$ for a computational domain of length $L = 600$. These values of numerical parameters were found to be a good compromise between accuracy and computational cost. In particular, the domain was specified long enough so that the numerical solution is not significantly affected by the periodic boundary conditions. Numerical tests on the conservation of invariants of motion will be shown in the next section. Note that the Hamiltonian formulation (8)~(9) together with the series expansion (11)~(13) of the DNO require that η be a single-valued graph of x .

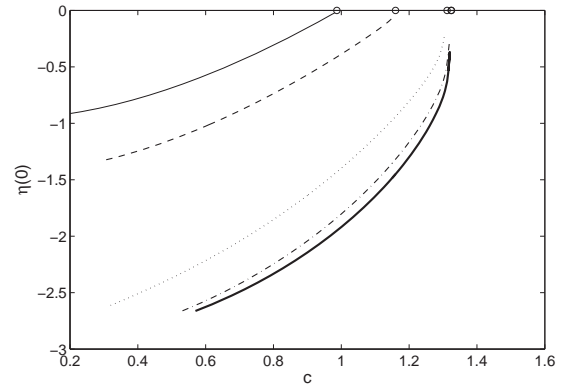


Figure 1: Amplitudes of depression solitary waves for $h = 1$ (thin solid line), $h = 1.5$ (dashed line), $h = 3.095$ (dotted line), $h = 5$ (dashed-dotted line) and $h = 8$ (thick solid line). The critical speed c_{\min} in each case is represented by a circle.

Numerical Results

In the steady case, we first compute solitary waves on infinite depth for $c < c_{\min}$ and then, by continuation, decrease the depth h . Depression and elevation solitary waves were found in all cases considered. Amplitude branches of depression solitary waves are presented in Fig. 1 for different values of h . For $h = 8$, the branch is very close to that in infinite depth and starts from a nonzero finite amplitude at $c = c_{\min}$. However, for $h = 1$ and $h = 1.5$, the wave amplitudes seem to approach zero at $c = c_{\min}$. Therefore, in shallow water, the solitary wave branches seem to start from zero amplitude while, in deeper water, they start at a finite amplitude. The exact critical depth where this change occurs cannot be easily found as it is difficult to accurately compute waves for values of c very close to c_{\min} (more and more oscillations appear and an increasingly larger number of grid points is needed).

In Fig. 2, we present a large-amplitude solitary wave with slightly overturning profile for $h = 3.095$. Such waves are found when c is small and for moderate to large depth. For large depth, the branch of depression solitary waves approaches a similar limiting profile. However, we were not able to follow this branch down to $c = 0$ because our solutions need to satisfy $x'(\phi) \rightarrow 1/c$ as $\phi \rightarrow \infty$, and thus the numerical scheme fails to yield accurate results for very small values of c .

We now turn our attention to the unsteady case and examine the regime $c > c_0$ where the 5th-order KdV equation (20) is applicable. For $h = 3.095$ and $P_0 = 0.1$, a solitary wave of elevation emerges in Fig. 3, which tends to separate at speed $c = 1.905$ from a large-scale radiative wavepacket induced by the initial forcing. Incidentally, a similar solution would develop if a negative pressure $P_0 = -0.1$ were applied. A close-up of this solitary wave of elevation is presented in Fig. 4 which compares it with a (numerical) solitary wave solution of (20). We set $\varepsilon = 1$ and only vary σ in (21)~(23) so that the iterative solution of (21) matches the fully nonlinear solitary wave as closely as possible. As in the context of gravity (or capillary-gravity) water waves, these 5th-order KdV solutions are so-called ‘generalized’ solitary waves in the sense that they are not truly localized but their central pulse typically connects to smaller periodic waves on both sides, as found in steady computations of Champneys et al. (2002). The wavelength $\ell_d = 2\pi/k_d$ of these dispersive

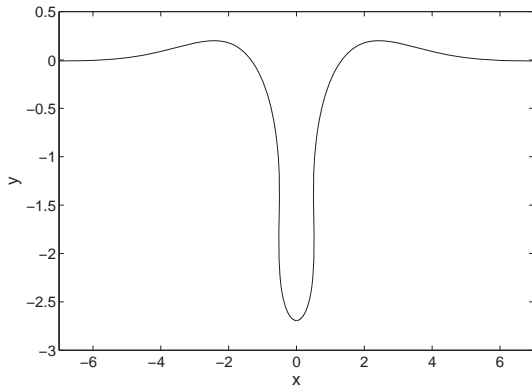


Figure 2: Large-amplitude overturning solitary wave for $c = 1.273$ and $h = 3.095$. Only the central part of the wave is shown.

tails is determined by the resonance condition

$$c_d(k_d) = \sqrt{h} \left[1 - \frac{1}{6} h^2 k_d^2 + \left(\frac{19}{360} h^4 + \frac{1}{2} \right) k_d^4 \right] = c, \quad (27)$$

where c_d is the 5th-order KdV approximation of (5) in dimensionless units. Solving (27) numerically yields $k_d = 0.586$ for e.g. $(c, h) = (1.905, 3.095)$, and it can be graphically checked in Fig. 4 that the dispersive wavelength is about $\ell_d = 2\pi/k_d = 10.714$ on both sides of the 5th-order KdV solitary wave. Figure 4 indicates a very good agreement for the central pulse in both amplitude and width. However, the fully nonlinear solitary wave seems to exhibit only one dispersive tail trailing behind it (i.e. on its left side). Despite the irregular unsteady shape of this dispersive tail, we see that its wavelength and amplitude are comparable to those in the 5th-order KdV solution. Such a low level of radiation may explain why this solitary wave of elevation seems to be steadily progressing, at least up to $t = 1000$. However, it is likely to be unstable as it gradually loses energy by emitting radiation.

As far as unsteady solutions are concerned, the occurrence of two dispersive tails is not possible in the present conservative case because otherwise this would imply that there is a wave source/sink at either $+\infty$ or $-\infty$. As mentioned in Michallet and Dias (1999), on which side the dispersive tail appears is determined by the value of its group velocity relative to that of its phase velocity. If the group velocity is less than the phase velocity, then ripples appear behind the solitary pulse. Otherwise, they appear ahead of it. In the present hydroelastic problem, the group velocity is less than the phase velocity if $k < k_{\min}$ and larger otherwise. Therefore, since $k_d = 0.586 < k_{\min} = 0.735$ for $(c, h) = (1.905, 3.095)$, ripples should trail behind the main pulse (i.e. on its left side), which is confirmed in Fig. 4 (lower panel).

On the other hand, for shallower water, say $(c, h) = (0.722, 0.5)$, we find $k_d = 0.501 > k_{\min} = 0.204$ and thus ripples are emitted ahead of the main crest (i.e. on its right side), as shown in Fig. 4 (upper panel). In this case again, the agreement is overall satisfactory between the 5th-order KdV and fully nonlinear solutions, modulo discrepancies due to unsteadiness in the latter. However, the fully nonlinear wave disperses more quickly than in the previous situation $h = 3.095$ because it emits a higher level of radiation. Note that the trough on the left side of the main crest is a remnant of the initial disturbance induced by the applied pressure (with $P_0 = 0.01$).

Finally, the conservation of invariants of motion (i.e. energy H , impulse I and volume V) after $t = T$ is illustrated in Fig. 5, for

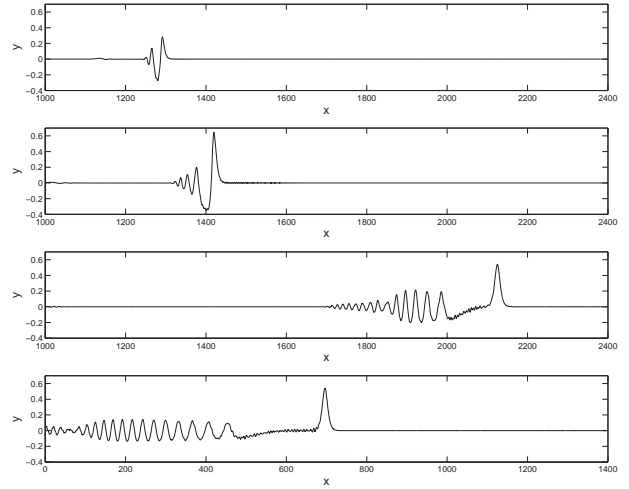


Figure 3: Snapshots of the ice-sheet deflection $\eta(x, t)$ at $t = 50, 120, 490, 1000$ (from top to bottom) for $P_0 = 0.1, c = 1.905$ and $h = 3.095$. The pressure is removed at $t = 125$. The high-order spectral method on the full equations (8)~(9) is used here.

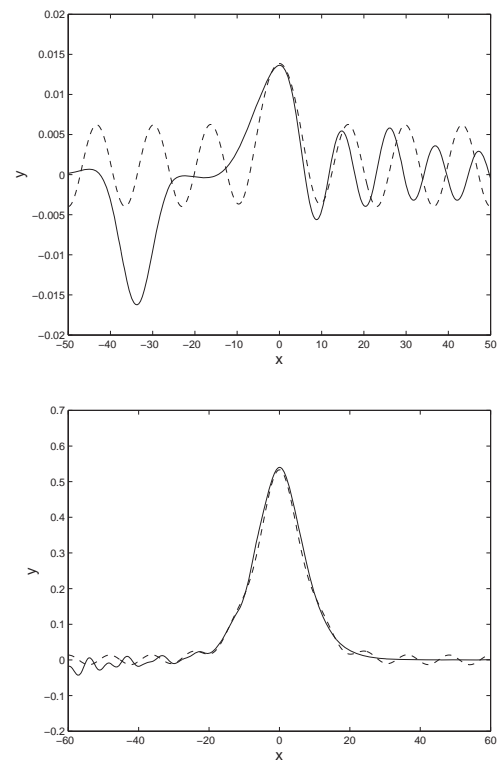


Figure 4: Comparison of wave profiles obtained from the high-order spectral method on (8)~(9) (solid line) and from the 5th-order KdV equation (20) (dashed line) at $t = 140$ for $(c, h) = (0.722, 0.5)$ (top) and at $t = 490$ for $(c, h) = (1.905, 3.095)$ (bottom).

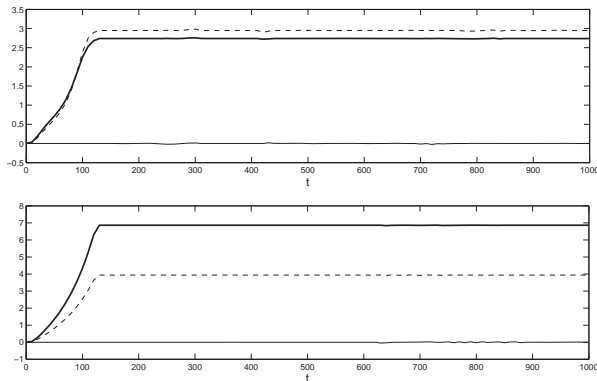


Figure 5: Time evolution of energy H (thick solid line), impulse I (dashed line) and volume V (thin solid line) for $(c, h) = (0.658, 1.5)$ (top) and $(1.905, 3.095)$ (bottom). The pressure is removed at $t = 125$.

$(c, h) = (0.658, 1.5)$ and $(1.905, 3.095)$. In both cases, we observe that these quantities are all very well conserved in time, with V being essentially zero as in the capillary-gravity water wave problem (Longuet-Higgins, 1989).

CONCLUSIONS

We have presented a Hamiltonian formulation for three-dimensional nonlinear flexural-gravity waves propagating at the surface of a finite-depth fluid covered by a continuous ice sheet. The ice cover is modeled as a thin elastic sheet, based on the special Cosserat theory of hyperelastic shells as proposed by Plotnikov and Toland (2011). The DNO is introduced to convert the original Laplace problem into a lower-dimensional system involving quantities evaluated only at the fluid-ice interface. We have used this Hamiltonian formulation to investigate the long-wave regime and derive a high-order KP equation for weakly nonlinear dispersive waves with large horizontal aspect ratio (i.e. slower variation in the transverse direction than in the longitudinal one). In the two-dimensional case, this asymptotic model reduces to a 5th-order KdV equation whose predictions compare well with direct numerical simulations of the full equations. For speeds near the shallow-water limit, fully nonlinear solitary waves of elevation resemble generalized solitary wave solutions of this 5th-order KdV equation, exhibiting a central pulse with a radiative tail. In the future, it would be of interest to perform direct numerical simulations of the three-dimensional problem and compare with predictions from our high-order KP equation. Preliminary three-dimensional computations were carried out by Părău and Vanden-Broeck (2011) for a linear Euler-Bernoulli model of the ice sheet combined with nonlinear potential flow.

ACKNOWLEDGEMENTS

P. Guyenne acknowledges support by the Simons Foundation through grant number 246170. E. I. Părău acknowledges support by the EPSRC through grant number EP/J019305/1. Both authors thank the Isaac Newton Institute for Mathematical Sciences (Cambridge, UK) for its hospitality during the Theory of Water Waves program in the summer

2014.

REFERENCES

- Biondini, G, and Chakravarty, S (2006). “Soliton solutions of the Kadomtsev–Petviashvili II equation,” *J Math Phys*, 47, 033514.
- Bonnefoy, F, Meylan, MH, and Ferrant, P (2009). “Nonlinear higher-order spectral solution for a two-dimensional moving load on ice,” *J Fluid Mech*, 621, 215-242.
- Champneys, AR, Vanden-Broeck, J-M, and Lord, GJ (2002). “Do true elevation gravity-capillary solitary waves exist? A numerical investigation,” *J Fluid Mech*, 454, 403-417.
- Craig, W, and Groves, MD (1994). “Hamiltonian long-wave approximations to the water-wave problem,” *Wave Motion*, 19, 367-389.
- Craig, W, Guyenne, P, and Kalisch, H (2005a). “Hamiltonian long wave expansions for free surfaces and interfaces,” *Comm Pure Appl Math*, 58, 1587-1641.
- Craig, W, Guyenne, P, Nicholls, DP, and Sulem, C (2005b). “Hamiltonian long wave expansions for water waves over a rough bottom,” *Proc R Soc Lond Ser A Math Phys Eng Sci*, 461, 839-873.
- Craig, W, Guyenne, P, and Sulem, C (2012). “The surface signature of internal waves,” *J Fluid Mech*, 710, 277-303.
- Craig, W, Schanz, U, and Sulem, C (1997). “The modulation regime of three-dimensional water waves and the Davey–Stewartson system,” *Ann Inst Henri Poincaré Anal Non Linéaire*, 14, 615-667.
- Craig, W, and Sulem, C (1993). “Numerical simulation of gravity waves,” *J Comp Phys*, 108, 73-83.
- Forbes, LK (1986). “Surface-waves of large amplitude beneath an elastic sheet. Part 1. High-order solutions,” *J Fluid Mech*, 169, 409-428.
- Guyenne, P, and Nicholls, DP (2007). “A high-order spectral method for nonlinear water waves over moving bottom topography,” *SIAM J Sci Comp*, 30, 81-101.
- Guyenne, P, and Părău, EI (2012). “Computations of fully nonlinear hydroelastic solitary waves on deep water,” *J Fluid Mech*, 713, 307-329.
- Guyenne, P, and Părău, EI (2014). “Finite-depth effects on solitary waves in a floating ice sheet,” *J Fluids Struct*, 49, 242-262.
- Haragus-Courcelle, M, and Ilichev, A (1998). “Three-dimensional solitary waves in the presence of additional surface effects,” *Eur J Mech B/Fluids*, 17, 739-768.
- Hegarty, GM, and Squire, VA (2008). “A boundary-integral method for the interaction of large-amplitude ocean waves with a compliant floating raft such as a sea-ice floe,” *J Eng Math*, 62, 355-372.
- Kaup, DJ (1975). “A higher-order wave equation and the method for solving it,” *Prog Theor Phys*, 54, 396-408.
- Kohout, AL, Williams, MJM, Dean, SM, and Meylan, MH (2014). “Storm-induced sea-ice breakup and the implications for ice extent,” *Nature*, 509, 604-607.
- Korobkin, A, Părău, EI, and Vanden-Broeck, J-M (2011). “The mathematical challenges and modelling of hydroelasticity,” *Phil Trans R Soc A*, 369, 2803-2812.
- Longuet-Higgins, MS (1989). “Capillary-gravity waves of solitary type on deep water,” *J Fluid Mech*, 200, 451-470.
- Marko, JR (2003). “Observations and analyses of an intense waves-in-ice event in the Sea of Okhotsk,” *J Geophys Res*, 108, 3296.
- Michallet, H, and Dias, F (1999). “Numerical study of generalized interfacial solitary waves,” *Phys Fluids*, 11, 1502-1511.
- Milewski, PA, Vanden-Broeck, J-M, and Wang, Z (2011). “Hydroelastic solitary waves in deep water,” *J Fluid Mech*, 679, 628-640.

- Milewski, PA, and Wang, Z (2013). "Three dimensional flexural-gravity waves," *Stud Appl Math*, 131, 135-148.
- Părău, E, and Dias, F (2002). "Nonlinear effects in the response of a floating ice plate to a moving load," *J Fluid Mech*, 460, 281-305.
- Părău, EI, and Vanden-Broeck, J-M (2011). "Three-dimensional waves beneath an ice sheet due to a steadily moving pressure," *Phil Trans R Soc A*, 369, 2973-2988.
- Plotnikov, PI, and Toland, JF (2011). "Modelling nonlinear hydroelastic waves," *Phil Trans R Soc A*, 369, 2942-2956.
- Squire, VA (2011). "Past, present and impendent hydroelastic challenges in the polar and subpolar seas," *Phil Trans R Soc A*, 369, 2813-2831.
- Squire, VA, Hosking, RJ, Kerr, AD, and Langhorne, PJ (1996). *Moving Loads on Ice Plates*, Kluwer, 45.
- Takizawa, T (1985). "Deflection of a floating sea ice sheet induced by a moving load," *Cold Reg Sci Tech*, 11, 171-180.
- Xia, X, and Shen, HT (2002). "Nonlinear interaction of ice cover with shallow water waves in channels," *J Fluid Mech*, 467, 259-268.
- Xu, L, and Guyenne, P (2009). "Numerical simulation of three-dimensional nonlinear water waves," *J Comp Phys*, 228, 8446-8466.
- Zakharov, VE (1968). "Stability of periodic waves of finite amplitude on the surface of a deep fluid," *J Appl Mech Tech Phys*, 9, 190-194.